JOURNAL OF MATERIALS SCIENCE 6 (1971) 1379–1388

Creep of CoO Single Crystals

A. H. CLAUER, M. S. SELTZER, B. A. WILCOX
Metal Science Group, Battelle Memorial Institute, Columbus Laboratories, 505 King Avenue, Columbus, Ohio 43201, USA

Cobalt monoxide single crystals having a [100] orientation were creep tested in compression over ranges of temperature, stress and oxygen pressure. The creep curves were S-shaped and only the inflection creep rate, $\dot{\epsilon}_2$, was analysed. In the range of 1000 to 1200°C, 850 to 1700 psi and 10^{-3} to 1 atm oxygen, $\dot{\epsilon}_2$ was given by

$$\dot{\epsilon}_2 = A\, p_{O_2}^{0.45}\, \sigma^{7.1} \exp(-Q_c/RT)$$

where $Q_c = 87 \pm 6$ kcal/mol at 0.01 atm O_2 and 100 ± 16 kcal/mol at 1 atm O_2. Slip occurred on two orthogonal $\{011\}\langle 0\bar{1}1\rangle$ slip systems. The presence of subboundaries was observed by optical and transmission electron microscopy. It is suggested that the creep rate is controlled by oxygen diffusion.

1. Introduction

The high temperature creep behaviour of oxides is of considerable interest for several reasons. Creep of oxide scales can be an important factor in maintaining a mechanically sound scale both during oxidation at high temperatures and during thermal cycling. Also, oxides will become increasingly important as structural materials when more is learned of their high temperature mechanical properties.

Grain size, purity, environment, stoichiometry, dispersions of other phases, and porosity all have a significant influence on the creep properties of oxides. The complications in interpreting creep mechanisms caused by the influence of grain boundaries and porosity on creep behaviour are greater in oxides than in metals. These can be avoided by first investigating the creep of single crystals. This investigation was undertaken to determine some of the pertinent factors controlling creep of CoO, including stoichiometry, temperature and stress.

2. Experimental Procedure

2.1. Materials

Two cobalt monoxide single crystal boules, grown by the flame fusion technique, were obtained from Marubeni-Iida (America), Inc. The boules had a [100] axial orientation and a typical manufacturer's analysis, in wt. %, was: 79.70 Co; 0.085 max Fe; trace Cu; 0.002 max Mn; 0.004 max Cl; 0.006 max SO_4; 0.0002 max Pb and other heavy metals.

A number of cylindrical creep specimens having a [100] axial orientation were ultrasonically trepanned from each boule. After machining, the end faces of the specimens were ground parallel on No. 600 SiC paper. The specimen dimensions were 0.16 in by 0.32 in long.

2.2. Creep Experiments

Creep experiments were performed in compression under a controlled atmosphere. The specimen was located in an alumina muffle tube which was sealed at both ends by water cooled "O" ring seals and bellows arrangements. The controlled atmosphere was provided by continuously flowing gases, consisting of air, pure oxygen, or argon-oxygen mixtures obtained commercially, and dried by passing them through Drierite. The temperature was controlled to within $\pm$ 2°C and the temperature gradient along the specimen was less than 1°C.

The loading platens in contact with the ends of the compression specimens were alumina, as were the loading ram and pedestal. No indentation of the loading platens by the specimen was ever detected. Sheets of 0.001 in thick platinum foil were placed between the specimen ends and the alumina in order to inhibit interaction between the CoO and Al_2O_3. This foil could be peeled off after most of the creep tests indicating very little or no interaction between the CoO specimen, platinum foil and alumina platens.

Specimens were loaded directly through the top loading ram and the stress was maintained

constant by adding the appropriate weights at 0.2% creep strain intervals. The upper load train was rigidly aligned by a set of linear bearings. Creep strain was recorded continuously during the creep test using a linear variable differential transducer (LVDT) to detect the difference in the deflection between the loading surfaces at the specimen. This arrangement provided a sensitivity of $\pm$ 60 microinches. No creep of the alumina push rods was observed at the highest temperature studied, 1200°C.

2.3. Microstructural Studies

Only surfaces parallel to {100} planes were examined metallographically. Specimens were cleaved on {100} planes parallel to the compression axis after creep. The specimens were then mounted and mechanically ground and polished. Most of the structural studies were made on the as-polished surfaces. Etch pitting studies were also made but the precipitation of a second phase, Co_3O_4, on cooling from the creep temperature modified the substructure formed during creep.

Thin foils for transmission electron microscopy (TEM) were prepared from creep tested specimens by first cleaving slabs on {100} planes parallel to the compression axis. The slabs were ground to 0.020 in. thickness and were subsequently jet indented chemically in H_2PO_4 maintained at 70 to 80°C. The thin areas at the periphery of the hole in the indented slab were then examined by TEM. Additional details of thin foil preparation are given in reference [1].

3. Results

Creep tests were conducted over a temperature range of 1000 to 1200°C and a stress range of 850 to 1700 psi. They were performed in atmospheres having controlled partial pressures of oxygen ranging from 1 to 10^{-4} atm.

The specimens were creep tested to only about 0.08 strain because barrelling of the specimen became significant at higher creep strains and made it impossible to maintain constant stress during creep. The cross-sections assumed an elliptical shape during creep, with the small diameter showing no change in dimension. After 0.08 creep strain, the strain in the centre of the gauge length was about 50% larger than the total compressive strain, causing the true stress in this region to decrease to 0.95 of the initial stress. This non-uniform deformation does not significantly affect the analysis of the creep results, since the creep parameters were determined for strains less than 0.04.

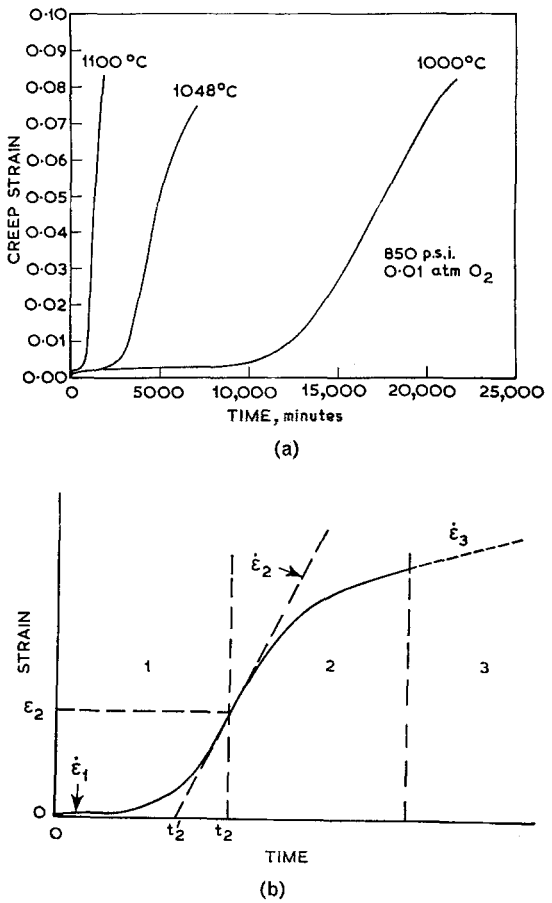

Figure 1 Typical creep curves and the creep curve notation. (a) Typical creep curves obtained at 850 psi and 1 atm oxygen at different temperatures. (b) Notation of the creep curve.

3.1. Creep Properties

The creep curves of all the crystals tested were sigmoidal (S-shaped), as shown in fig. 1. The CoO single crystals exhibited only stages 1 and 2 of the three-stage sigmoidal creep curve shown in fig. 1b. Stage 1 consisted of an inflection in the creep curve shortly after loading, followed by a region in which the creep rate increased with increasing creep strain. The initial inflection, having a slope, $\dot{\epsilon}_1$, resulted from the creep rate decreasing immediately after loading before it began to increase with increasing creep strain. Stage 2 is a region of continuously decreasing creep rate with increasing creep strain. The creep rate at the inflection in the creep curve

dividing regions 1 and 2 is designated $\dot{\epsilon}_2$. Stage 3, corresponding to steady state creep, with a constant creep rate, was not observed up to 0.085 creep strain. Presumably it would have been present at higher creep strains if the effects of barrelling had been removed and the creep test continued [2]. The quantities ϵ_2, t_2, and t_2' in fig. 1b have often been used in describing sigmoidal creep curves, and they are included in the summary of the creep results in table I. The terms ϵ_2 and t_2 are the strain and time of the second inflection, respectively.

Sigmoidal creep curves have often been observed in non-metallic single crystals during creep, e.g., Ge [3, 4], Si [5], InSb [6], LiF [7, 8], doped AgBr [2], NaCl [9], UO_2 [10], Al_2O_3 [11], and FeO [12]. Although a rate corresponding to $\dot{\epsilon}_1$ has not been reported, this may be a characteristic of the sensitivity of the strain measuring devices used previously.

In the absence of a steady state creep rate, $\dot{\epsilon}_3$, and because of the wide scatter and low values of $\dot{\epsilon}_1$, only the creep rate $\dot{\epsilon}_2$ was used to characterise the creep behaviour of the CoO crystals. Considerable variations in the values of $\dot{\epsilon}_2$ were observed between specimens from the two boules. The scatter was minimised significantly by comparing only specimens from the same boule. The temperature and stress dependence of $\dot{\epsilon}_2$ was determined using only specimens from Boule 2. Specimens from both boules were compared in determining the oxygen pressure dependence of $\dot{\epsilon}_2$.

The temperature dependence of $\dot{\epsilon}_2$ was measured at a constant stress of 850 psi and at two oxygen pressures, 1 and 0.01 atm, and is shown in fig. 2. Activation energies of $Q_c = 100 \pm 16$ kcal/mol and 87 ± 6 kcal/mol at $p_{O_2} = 1$ and 0.01 atm, respectively, were derived. The probable error ranges overlap and it is not certain that Q_c decreases with decreasing oxygen pressure.

The stress dependence of $\dot{\epsilon}_2$ is shown in fig. 3 for $p_{O_2} = 1$ atm and a test temperature of 1000°C. The results can be represented by a power law, $\dot{\epsilon}_2 \propto \sigma^n$, where the least squares fit to the points gives $n = 7.1 \pm 0.1$. This is within the range of values reported for single crystals of other ionic compounds with the NaCl crystal structure, e.g., $n = 5.6$ for NaCl using the replotted data of Illschner and Reppich [9], and $n = 8.4$ to 10.1 for LiF [8]. These in turn differ from the results for single crystals of covalently bonded materials with the diamond structure,

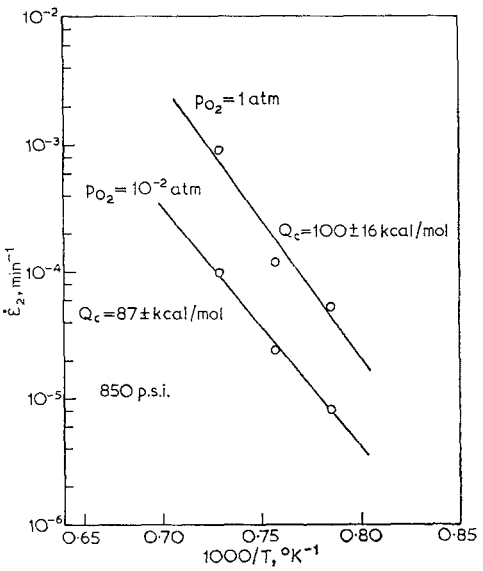

Figure 2 The temperature dependence of $\dot{\epsilon}_2$ at two oxygen pressures. All of the specimens are from Boule 1.

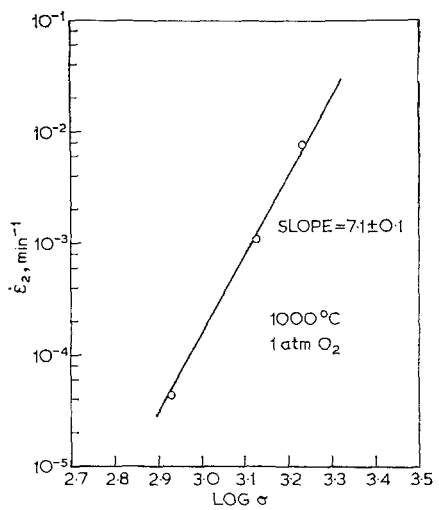

Figure 3 The stress dependence of $\dot{\epsilon}_2$ at one atmosphere of oxygen. All of the specimens are from Boule 1.

for which $n = 3.3$ in Ge [13], 3.3. in InSb [6] and 3.0 in Si [5]. However, the higher stress exponent for CoO is in accord with the tendency for ionic crystals to have larger exponents than the covalently bonded crystals.

The p_{O_2} dependence of $\dot{\epsilon}_2$ is shown in fig. 4. Over the range 1 atm $\gtrsim p_{O_2} \gtrsim 10^{-3}$ atm, $\dot{\epsilon}_2$ decreases with decreasing p_{O_2}. The results from both boules are shown separately. Temperature compensated creep rates were plotted, assuming a constant value of $Q_c = 94$ kcal/mol independ-

ent of oxygen pressure. However, the creep rates from specimens tested at varying p_{O_2} at a constant temperature, 1100°C, give nearly the same slopes as those in fig. 4. The absence of large deviations in fig. 4 over the p_{O_2} range 10^{-3} to 1 atm indicates that Q_c varies less than 10 kcal/mol over this range. If Q_c does decrease with decreasing p_{O_2}, then the slope determined from fig. 4 is too large. Also, the oxygen-pressure dependence would decrease with decreaing temperature. The more extensive data from Boule 2 were fitted by a least mean squares analysis to give a power law rate dependence, $\dot{\epsilon}_2 \propto p_{O_2}{}^m$, where $m = 0.45 \pm 0.02$. A parallel line was drawn through the data from Boule 1.

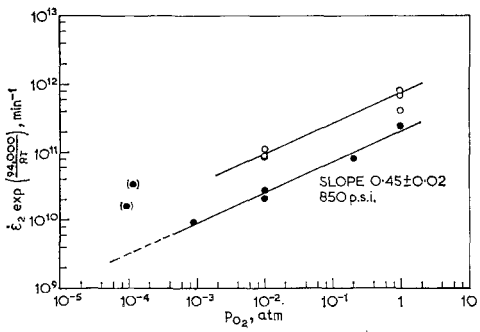

Figure 4 The dependence of the temperature compensated creep rate, $\dot{\epsilon}_2$, on the oxygen pressure. The open circles are from Boule 1, shown in figs. 2 and 3, and the filled circles are from Boule 2. The points designated by () are discussed in the text.

The points at $p_{O_2} \cong 10^{-4}$ atm enclosed in parenthesis in fig. 4 are significantly above the line representing $\dot{\epsilon}_2 \propto p_{O_2}{}^{0.45}$. This could be a real effect wherein the creep rate became independent of the oxygen pressure at low p_{O_2}. However, there was also a possibility that the specimens at $p_{O_2} = 10^{-4}$ atm were not at the equilibrium composition during creep. The reason for this is clear from the phase diagram of Fisher and Tannhauser [14]. For $Co_{1-x}O$ at 1100°C and $p_{O_2} = 1$ atm, x $\cong$ 0.008, whereas at $p_{O_2} = 10^{-4}$ atm, x $\cong$ 0.0008. Thus, there are ten times as many cobalt vacancies available for diffusion at $p_{O_2} = 1$ atm than at $p_{O_2} = 10^{-4}$ atm. This makes the approach to equilibrium composition much slower as the stoichiometric composition is approached at lower p_{O_2}. The as-received specimens have a large amount of Co_3O_4 precipitate, i.e., a large deviation from stoichiometry. Thus, if the equilibrium composition was not reached at 10^{-4} atm O_2, the average compositions of these two specimens would be equivalent to a composition in equilibrium with a higher p_{O_2}, in which case the two data points in fig. 4 corresponding to $p_{O_2} = 10^{-4}$ atm would be shifted to the right.

The difference in creep behaviour between Boules 1 and 2 is obvious in fig. 4. The spacings between the curves in fig. 4 show that creep rates from Boule 1 are a factor of 3.8 faster than those from Boule 2. An optical emission analysis was performed on each boule to determine whether the difference in creep properties between the boules was due to impurities. The levels of impurities in each boule were identical within the accuracy of the technique. The results of the analysis in wt. % were Si, 0.001-0.002; Mn, 0.02; Fe, 0.05; Mg, 0.01; Al, 0.008; Cu, trace; Ni, 0.1; Ca, 0.003; other elements were sought but not found. Therefore any impurity effect must be attributed to a difference in concentration of impurities below the level of the sensitivity of this method of analysis. A difference in the grown-in dislocation substructure could also have been responsible for the difference in creep strength of the two boules, but such a variation could not be observed.

In accord with this study, Strafford and Gartside [15] observed that the steady state bending creep rate, $\dot{\epsilon}_s$, increased with increasing p_{O_2} in polycrystalline CoO scales. However, the creep rate was not very sensitive to p_{O_2}, being $\dot{\epsilon}_s \propto p_{O_2}{}^m$ where $m \cong 0.15$ over the range 10^{-2} atm $\leq p_{O_2} \leq 1$ atm. Similarly, in polycrystalline $Fe_{1-x}O$, $\dot{\epsilon}_s \propto p_{O_2}{}^{0.21}$ [16].

3.2. Deformation Mode

The operative slip direction in crystals having the sodium chloride crystal structure is predominantly ⟨110⟩, although ⟨100⟩ has been reported in PbS [17] and PbTe [18]. The primary slip planes are {110} and {100}, although {111} slip planes have been reported under certain conditions [19]. The slip systems operating during compression creep in this investigation could not be identified directly since the slip lines were not visible after creep in uniformly compressed specimens. However, one specimen sheared by a relative sideways displacement of its end faces because of misalignment. The slip lines were visible in this specimen as shown in fig. 5. In fig. 5a the slip lines are straight and there are large offsets on the right and left sides of the specimen, indicating that screw dislocations emerged through the (100) plane and the slip

TABLE I Summary of Creep Data for CoO Single Crystals (See fig. 1b for explanation of symbols)

Boule[a] Number	Stress, psi	Temperature °C	Oxygen Pressure, atm	$\dot{\epsilon}_2$, min^{-1}	ϵ_2	t_2, min	t_2' min
2	850	1000	1.0	5.2×10^{-5}	—	—	—
2	850	1048	1.0	$\sim 1.2 \times 10^{-4}$	0.024	950	~ 750
2	850	1100	1.0	9.2×10^{-4}	0.0265	84	54
1	850	1157	1.0	1.06×10^{-3}	0.019	30	12
2	850	1000	1×10^{-2}	$\sim 9 \times 10^{-6}$	(0.038)[b]	(16,300)[b]	$\sim 12{,}500$
2	850	1048	1×10^{-2}	2.4×10^{-5}	(0.034)[b]	(4,300)[b]	2,900
2	850	1100	1×10^{-2}	9.8×10^{-5}	(0.037)[b]	1,220	840
1	850	1157	1×10^{-2}	9.0×10^{-5}	(0.03)[b]	662	330
1	850	1200	1×10^{-2}	3.14×10^{-4}	0.026	300	218
1	1075	1000	1.0	2.2×10^{-4}	0.0225	550	448
2	1330	1000	1.0	1.07×10^{-3}	0.024	135	12.5
2	1700	1000	1.0	7.6×10^{-3}	0.0265	8.9	5.4
1	850	1100	0.21 [air]	9.0×10^{-5}	0.0275	820	500
1	850	1100	8.9×10^{-4}	1.02×10^{-5}	0.0245	8,000	5,600
1	850	1100	9.4×10^{-5}	1.75×10^{-5}	0.029	6,600	4,900
1	850	1100	1.15×10^{-4}	3.7×10^{-5}	—	—	—

[a] The number, 1 or 2, identifies which of the boules the specimens came from.
[b] () signifies that these are approximate values.

direction is parallel to this surface. In fig. 5b the slip lines are wavy and there are no distinguishable offsets on the right and left sides of the specimen, indicating that edge dislocations emerged through the (010) plane. Since the specimen axis is a $\langle 001 \rangle$ direction and the photographs are parallel to $\{100\}$ planes, the slip system in fig. 5 is a $\langle 011 \rangle \{0\bar{1}1\}$ system.

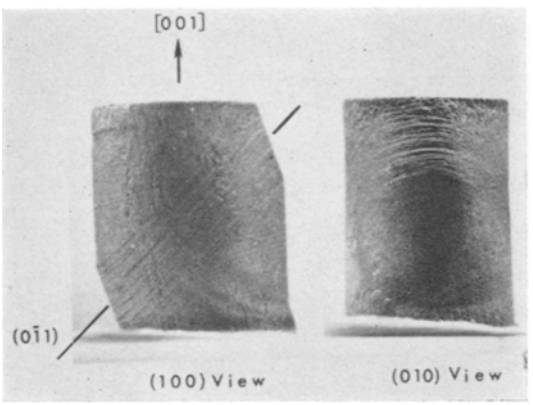

Figure 5 Slip bands on an atypical specimen that deformed predominantly by slip on one slip system (× 9).

The elliptical cross section developed in the symmetrically deformed specimens is consistent with two orthogonal $\{011\}\langle 0\bar{1}1\rangle$ slip systems operating under these conditions. The simultaneous operation of the slip system $[011](0\bar{1}1)$, evident in fig. 5, and the symmetric slip system, $[0\bar{1}1](011)$, would produce the observed shape change in the specimens which deformed "normally".

3.3. Creep Substructure

The dislocation substructure developed during creep could not be observed in detail because of the local deformation introduced around particles of Co_3O_4 which precipitated during cooling (below $\sim 900°C$) from the creep temperature. Examination by etch pitting and transmission electron microscopy, verified that large numbers of dislocations were introduced by these particles [1]. Because of the particles the creep substructure was studied on mechanically polished $\{100\}$ surfaces by relying on decoration of sub-boundaries or groups of dislocations by the Co_3O_4 precipitates. This was not completely satisfactory, but it did reveal some details of the creep substructure. The as-received crystals rarely showed decorated sub-boundaries.

A specimen creep tested at a high stress, 1700 psi, formed sub-boundaries during creep as shown in fig. 6. The two plane trace analysis of fig. 6 indicates that the rows of particles represent planes parallel to $(0\bar{1}1)$. The specimen orientation was indexed relative to the specimen shape after creep, with the compression axis parallel to [001] and the major axis of the cross-section parallel to [010].

A regular array of sub-boundaries predominantly parallel to the traces of two perpendicular

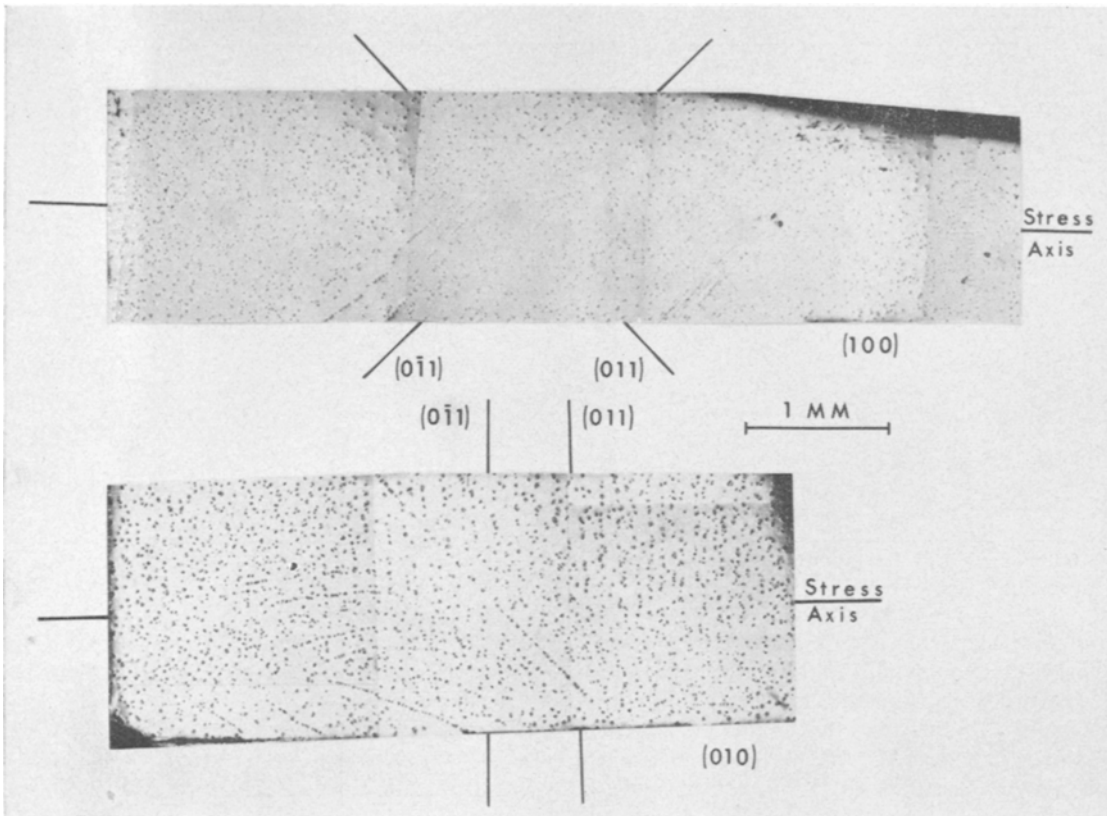

Figure 6 Sub-boundaries decorated with Co_3O_4 particles after creep at a high stress, 1700 psi, and 1000°C in a 1.0 atm oxygen. The total creep strain was 0.082.

{110} planes is shown in fig. 7. This specimen was creep tested at a lower stress, 930 psi. Since this is a (100) surface, the traces are parallel to the traces of the (0$\bar{1}$1) and (011) planes.

Most of the decorated, regular boundaries formed during creep were parallel to (0$\bar{1}$1) or (011) planes. Also, the spacing between the decorated boundaries decreased with increasing stress as seen in figs. 6, 7. These planes are both active slip planes and tilt boundary planes. However, if the glide planes were so well defined by a high density of glide dislocations that they were preferentially decorated by the Co_3O_4 precipitate, it would be expected that large slip offsets would be visible on the surface with a spacing between them comparable to the spacing between the decorated boundaries. This has been observed in high temperature creep of molybdenum single crystals [20]. Except for those in fig. 5, heavy slip bands were not observed in the CoO single crystals.

Also, sub-boundaries were observed by TEM in creep tested CoO single crystals as shown in fig. 8. The boundaries were well away from large Co_3O_4 particles, making it probable that most of the dislocations in the boundaries originated during creep. However, some were undoubtedly created by particles, so that a Burger's vector determination was not made. Therefore, it is most likely that the precipitates are decorating sub-boundaries which are predominantly tilt boundaries, rather than decorating slip planes.

The conditions under which the boundaries formed are not clear. These sub-boundaries are representative of the final creep strain and thus represent a strain approaching the steady state creep region. Therefore, it is not unexpected that the sub-boundaries would be a relaxed configuration such as tilt boundaries. Of a series of specimens creep tested at $p_{O_2} = 1$ atm and 1000°C, only the specimens tested at 850 and 1700 psi contained decorated sub-boundaries. The absence of decorated sub-boundaries after creep at 1075 and 1330 psi may be due to either a

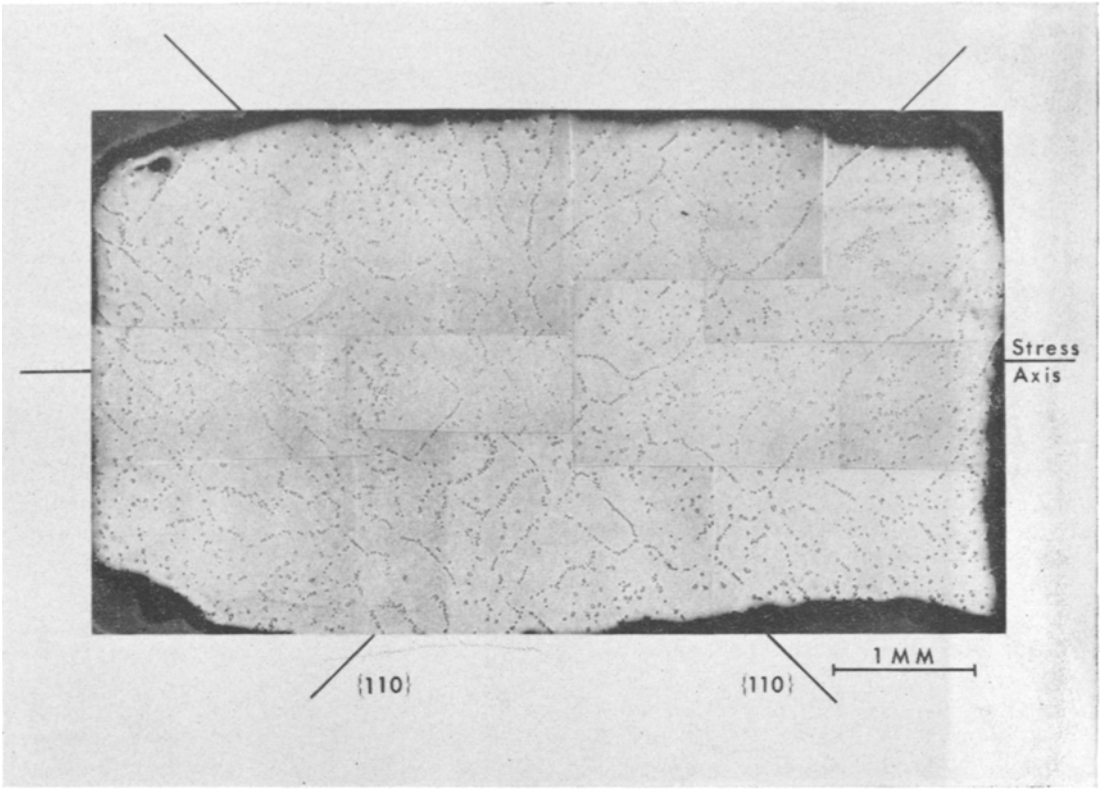

Figure 7 A {100} surface containing two sets of sub-boundaries with Co_3O_4 precipitates. The specimen was creep tested at 1100°C in 1.0 atm oxygen. The stress was increased during the test and the final stress was 930 psi. The total creep strain was 0.086.

failure of the decoration process or the absence of sub-boundaries. It was presumed that a straightforward relation between the substructure and slip could be obtained from an examination of the substructure in the specimen shown in fig. 5. However, the precipitates on longitudinal sections did not exhibit any discernable substructural pattern.

4. Discussion

The activation energy for high temperature creep of binary compounds suggests that often creep is diffusion controlled. Although this usually refers to the steady state creep rate in region 3 of fig. 1b, it also appears to apply to $\dot{\epsilon}_2$. Diffusion rates for cobalt [21, 22] and oxygen [23-25] in CoO have been measured. At 0.2 atm oxygen pressure Carter and Richardson [21] found the cobalt diffusion activation energy to be 34.5 kcal/mol, and the diffusivities increased as $p_{O_2}{}^{0.3}$ at 1150°C in the region 10^{-3} to 1 atm p_{O_2}. Chen, *et al.* [22], found the cobalt diffusion activation energy to be 38.4 kcal/mol in air. Chen and Jackson [25] found an activation energy for oxygen diffusion of 95 kcal/mol at 0.21 atm oxygen. From these studies, diffusivities at 1150°C and 0.2 atm p_{O_2} of 3 to 6 $\times$ 10^{-9} cm^2/sec for cobalt and 1.2 $\times$ 10^{-13} cm^2/sec for oxygen can be determined. The partial pressure dependence of the oxygen diffusion rate in CoO has not been determined. The studies by Holt [24], who used the proton activation technique, and by Chen and Jackson [25], who used the isotopic exchange method, are in excellent agreement, and it is believed that they are most representative of bulk diffusion of oxygen in CoO.

Diffusion controlled high temperature creep of binary compounds is considered to be limited by the migration of the slower diffusing compound constituent. The oxygen diffusion rates are at least four orders of magnitude lower than

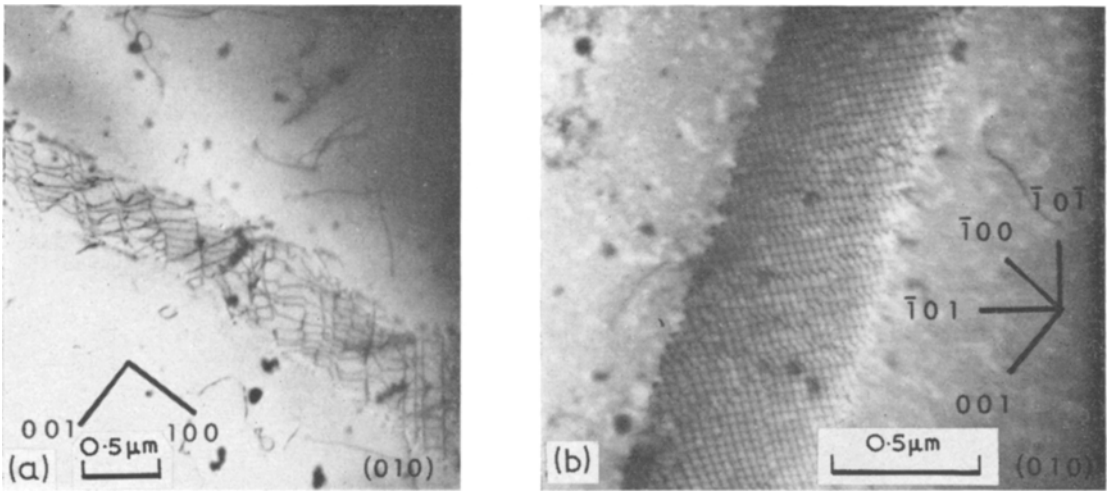

Figure 8 Two types of sub-boundaries observed in CoO after creep. (a) Creep tested at 1000° C and 1700 psi in one atm oxygen to 0.082 creep strain. (b) Creep tested at 1048° C and 850 psi in 0.01 atm oxygen to 0.077 creep strain. The misorientation across the boundary is 0.4° around [100].

the cobalt diffusivities at 1150° C and 0.2 atm oxygen pressure. Also, the values for Q_c at 10^{-2} and 1 atm oxygen, 87 and 100 kcal/mole, respectively, bracket the oxygen diffusion activation energy of 95 kcal/mole determined at 2×10^{-1} atm, and are much greater than the cobalt diffusion activation energy of 34.6 kcal/mol. This correlation suggests that high temperature creep of CoO single crystals under these conditions is controlled by oxygen diffusion, although the agreement may be fortuitous.

S-shaped creep curves have been observed in metals, compounds and semiconductor materials. However, the mechanisms causing this particular creep behaviour are probably not the same in many cases, and they have not been well characterised except for the diamond structure semiconductors by Hassen and co-workers [5, 6, 26]. The general characteristics of the deformation mechanisms causing this behaviour are a low initial mobile dislocation density and/or mobility which subsequently increase with time under load to a maximum at the inflection in the creep strain-time curve. After the inflection in the creep curve, there is a decrease in dislocation mobility caused by the high density of accumulated dislocations.

The general models for describing the S-shaped creep curve [6, 26-29] and in particular, $\dot{\epsilon}_2$, either do not consider recovery mechanisms or do not differentiate between immobilisation or annihilation of dislocations. However, at high temperatures, recovery due to rearrangement and annihilation of dislocations could be very important over the entire creep curve, and not just after the inflection where the regular subgrain structure shows it is prevalent. In the models, $\dot{\epsilon}_2$ is proportional to the dislocation glide velocity and some function of a work hardening parameter. In the absence of recovery, the temperature dependence of the work hardening parameter for a given type of dislocation structure will be principally that of the shear modulus and will therefore be only a minor contribution to the temperature dependence of $\dot{\epsilon}_2$ for the usual range of activation energies for creep. If significant recovery occurs through the inflection point, the situation is much more complex.

Without being able to make a detailed study of the dislocation substructure developing during creep to test the theoretical models quantitatively, the S-shaped creep curves in the CoO single crystals cannot be unambiguously interpreted. Hence, the creep curves will only be discussed briefly in general terms. If recovery processes are not significant during the early stages of creep, then $\dot{\epsilon}_2$ is approximately proportional to the dislocation glide velocity. Possible oxygen diffusion controlled glide mechanisms are the glide of jogged screws [30] and the glide of charged dislocations dragging an atmosphere of charged defects [31]. At the low stress levels used here these are viscous glide mechanisms, i.e., glide velocity, $v \propto \sigma$.

However, the observed stress dependence, $\dot{\epsilon}_2 \propto \sigma^{7.1}$, is too large to fit the viscous glide models, for which $\dot{\epsilon}_2 \propto \sigma^n$ where $n = 2$ [27] or 3 [26] and thus these models will not suffice. The higher stress dependence indicates either that both recovery and glide processes are operative which increase the stress dependence but are both oxygen diffusion controlled, such as recovery by dislocation climb, or that the apparent agreement between Q_c and Q_D of oxygen is fortuitous.

For the simpler case where $Q_c = Q_D$ of oxygen, the mechanism of oxygen migration is now considered. Oxygen can migrate via either simple, unassociated defects or via numerous types of complex point defects which can include either oxygen interstitials or vacancies and can be neutral or ionised. If the simplest possibility is examined and it is assumed that unassociated point defects predominate at the temperatures employed in this study, the two possibilities are: (1) diffusion via vacancies in the oxygen sublattice or (2) interstitial diffusion of oxygen. It has been shown that $\dot{\epsilon}_2 \propto p_{O_2}{}^{0.45}$ in the range 10^{-3} to 1 atm. This result suggests that oxygen interstitial diffusion is the rate controlling process, since the concentration of oxygen vacancies decreases with increasing oxygen partial pressure while the concentration of oxygen interstitials is an increasing function of p_{O_2}.

In CoO the predominant defects are cobalt vacancies [14]. At high oxygen pressures the neutrality condition is $[e^+] = [V_{Co}{}']$ where $[e^+]$ and $[V_{Co}{}']$ are the concentrations of electron holes and singly ionised cobalt vacancies, respectively. At low oxygen pressures the neutrality condition is $[e^+] = 2[V_{Co}{}'']$ where $[V_{Co}{}'']$ is the concentration of doubly ionised cobalt vacancies. The primes represent negative charge.

Following the notation of Kröger and Vink [32], the pressure dependence of the different concentrations of oxygen interstitials is as follows:

$$[O_i{}^x] \propto p_{O_2}{}^{1/2}, \quad (1)$$

independent of the neutrality condition,

$$[O_i{}'] \propto p_{O_2}{}^{1/4}; \text{ and } [O_i{}''] = \text{constant}, \quad (2)$$

for $[e^+] = [V_{Co}{}']$, and

$$[O_i{}'] \propto p_{O_2}{}^{1/3}; \text{ and } [O_i{}''] \propto p_{O_2}{}^{1/6}, \quad (3)$$

for $[e^+] = 2[V_{Co}{}'']$, where $[O_i{}^x]$, $[O_i{}']$ and $[O_i{}'']$ are concentrations of neutral, singly ionised, and doubly ionised interstitials, respectively. Examination of the above equations shows that a pressure dependence of oxygen interstitials close to $p_{O_2}{}^{0.45}$ is possible only if neutral oxygen interstitials control the creep.

While the results of this study are the first to suggest the existence of oxygen interstitials in CoO, investigations of oxygen diffusion in a number of other oxide systems have found that oxygen diffusion increases with increasing oxygen pressure in NiO [33], Cu_2O [34], and ZnO [35]. The possibility that oxygen diffuses as an interstitial defect in oxides is often dismissed on the basis of size considerations, e.g., oxygen as O'' has an ionic radius of 1.32Å. However, neutral oxygen has a radius of 0.60Å and may be expected to migrate with relative ease through CoO.

5. Conclusions

1. ⟨100⟩ oriented CoO single crystals exhibited S-shaped creep curves in compression.
2. The activation energy for the creep rate at the inflection of the creep curve, $\dot{\epsilon}_2$, was 87 ± 6 kcal/mol at $p_{O_2} = 0.01$ atm and 100 ± 16 kcal/mol at $p_{O_2} = 1.0$ atm. These values are in good agreement with the activation energy for self diffusion of oxygen in CoO, 95 kcal/mol at $p_{O_2} = 0.2$ atm [33].
3. The stress dependence of $\dot{\epsilon}_2$ was $\dot{\epsilon}_2 \propto \sigma^{7.1 \pm 0.1}$.
4. The oxygen pressure dependence of $\dot{\epsilon}_2$ was $\dot{\epsilon}_2 \propto p_{O_2}{}^{0.45 \pm 0.02}$ for $10^{-3} < p_{O_2} < 1$ atm.
5. Slip was observed on slip systems of the type $\langle 011 \rangle \{0\bar{1}1\}$.
6. Sub-boundaries formed during creep were observed after decoration with Co_3O_4 precipitates. These boundaries were parallel to {011} planes and may be either tilt or glide boundaries.

Acknowledgements

The able technical assistance of M. R. Cantin, J. R. Bibler, and the late R. D. Tenaglia is gratefully acknowledged. The authors are indebted to A. Z. Hed for valuable discussions. This research was sponsored by the National Aeronautics and Space Administration under Grant NGR-36-002-070.

References

1. M. R. CANTIN, A. H. CLAUER, M. S. SELTZER, and B. A. WILCOX, *J. Amer. Ceram. Soc.* **52** (1969) 112.
2. R. W. CHRISTY, *Acta Metallurgica* **2** (1954) 284.
3. J. R. PATEL and B. H. ALEXANDER, *ibid.* **4** (1956) 385
4. D. DEW HUGHES, *IBM Journal*, **45** (1961) 279.
5. B. REPPICH, P. HAASEN, and B. ILLSCHNER, *Acta Metallurgica* **12** (1964) 1283.
6. E. PEISSKER, P. HAASEN, and H. ALEXANDER, *Phil. Mag.* **7** (1961) 1279.

7. W. G. JOHNSTON, *J. Appl. Phys.* **33** (1962) 2716.
8. W. A. COGHLAN, Ph.D. dissertation, Stanford University, 1969.
9. B. ILSCHNER and B. REPPICH, *Phys. Stat. Sol.* **3** (1963) 2093.
10. W. M. ARMSTRONG, A. R. CAUSEY, and W. R. STRURROCK, *J. Nucl. Mater.* **19** (1966) 42.
11. J. B. WACHTMAN and L. H. MAXWELL,, *J. Amer. Ceram. Soc.* **40** (1957) 377.
12. B. REPPICH, *Phys. Stat. Sol.* **20** (1967) 69.
13. J. HEWING, Diplomarbeit Göttingen, from P. HAASEN, *NPL Symp.*, The Relation Between Structure and Mechanical Properties of Metals (HMSO, London, 1963).
14. B. FISHER and D. S. TANNHAUSER, *J. Electrochem. Soc.* **111** (1964) 1194.
15. K. N. STRAFFORD and H. GARTSIDE, *J. Mater. Sci.* **4** (1969) 760.
16. B. ILSCHNER, B. REPPICH, and E. RIEKE, *Discuss. Faraday Soc.* **38** (1964) 243.
17. M. J. BUERGER, *Amer. Min.* **15** (1930) 36.
18. W. A. RACHINGER, *Acta Metallurgica* **4** (1956) 647.
19. J. P. HIRTH and J. LOTHE, "Theory of Dislocations" (McGraw-Hill Book Co., New York, 1968) 269.
20. A. H. CLAUER, B. A. WILCOX, and J. P. HIRTH, *Acta Metallurgica* **18** (1970) 381.
21. R. E. CARTER and F. D. RICHARDSON, *Trans. AIME*, **200** (1954) 1244.
22. W. K. CHEN, N. L. PETERSON, and W. T. REEVES, *Phys. Rev.*, **186** (1969) 887.
23. B. A. THOMPSON, Ph.D. dissertation, Rensselaer Polytechnic Institute, 1962, (University Microfilms, Ann Arbor, Michigan, 1963).
24. J. B. HOLT, *Proc. Brit. Ceram. Soc.* (1967) 157.
25. W. K. CHEN and R. S. JACKSON, *J. Phys. Chem. Solids*, **30** (1969) 1309.
26. P. HAASEN, "Dislocation Dynamics", Ed. A. R. Rosenfield, G. T. Hahn, A. L. Bement, and R. I. Jaffee (McGraw-Hill Book Co., New York, 1968) 701.
27. G. A. WEBSTER, *Phil. Mag.* **14** (1966) 775.
28. J. J. GILMAN, *J. Appl. Phys.* **36** (1965) 2772.
29. W. G. JOHNSTON, *ibid* **33** (1962) 2716.
30. N. F. MOTT, "Creep and Fracture of Metals at Elevated Temperatures" (HMSO, London, 1956) 21.
31. J. D. ESHELBY, C. W. A. NEWEY, P. L. PRATT, and A. B. LIDIARD, *Phil. Mag.* **3** (1958) 75.
32. F. A. KRÖGER and H. J. VINK, *Sol. State Phys.* **3** (1956) 307.
33. M. O'KEEFE and W. J. MOORE, *J. Phys. Chem.* **65** (1961) 1438.
34. W. J. MOORE, Y. EBISUZAKI, and J. A. SLUSS, *ibid* **62** (1958) 1438.
35. W. J. MOORE, and E. L. WILLIAMS, *Discuss. Faraday Soc.* **28** (1959) 86.

Received 29 March and accepted 6 July 1971.